

# Effect of thickness on structural, electrical, and spectral response properties of thermal evaporated CdTe films

V K Ashith<sup>1</sup>, K Priya<sup>2</sup> and G K Rao<sup>2\*</sup> 

<sup>1</sup>Department of Physics, St. Philomena College, Puttur, Karnataka 574202, India

<sup>2</sup>Department of Physics, Manipal Institute of Technology, Manipal Academy of Higher Education, Manipal, Karnataka 576104, India

Received: 01 December 2021 / Accepted: 10 September 2022 / Published online: 1 October 2022

**Abstract:** The II–VI semiconductor thin films have vast applications in optoelectronics. Cadmium telluride (CdTe) is one such material, which has proved to be useful in the fabrication of solar cells, photodetectors, etc. In the present work, CdTe thin films have been deposited on glass substrates by thermally evaporating CdTe powder under a high vacuum. The optimum film thickness for photovoltaic applications was determined by performing a detailed characterization of the films. The thermal evaporated CdTe films were found to be polycrystalline with a cubic structure. Considerable improvement in the crystallinity was observed with the increase in thickness. The lattice constant, dislocation density, strain, and stress have also been analyzed. The optical properties of the CdTe films have been observed to change with thickness. The maximum optical absorption was found in the near infrared region. The photoluminescence spectra showed a prominent peak, corresponding to the band-edge transition of the CdTe films. The electrical properties of the films were found to improve with thickness. The films yield maximum photocurrent at 820 nm. Based on the detailed characterization, the film thickness of 950 nm was found to be most suitable for photovoltaic application.

**Keywords:** II–VI semiconductors; Vacuum deposition; Thickness; Crystallite size; Spectral response

## 1. Introduction

In the current scenario, thin-film technology is one of the most promising fields for energy-efficient optoelectronics and renewable energy research. The technology has tremendous applications from the device fabrication point of view [1, 2]. Among the semiconductor thin films, the II–VI semiconductors have enormous advantages due to their direct band gaps which cover the NIR-VIS-UV region of the electromagnetic spectrum. Cadmium telluride (CdTe) is one such II–VI semiconductor, with a high absorption coefficient and a direct energy bandgap of 1.45 eV, which is most suitable for the fabrication of photovoltaic devices [3–7]. Often, the as-deposited CdTe thin films exhibit p-type conductivity. However, it can also be obtained in n-type form by suitably altering the deposition process [8, 9]. The p-type CdTe thin films have been successfully utilized in CdS/CdTe and ZnS/CdTe heterojunction solar

cells [10, 11]. Apart from the solar cells, the CdTe thin films can also be used to fabricate LEDs, IR-Photodetectors, and other optoelectronic devices [12, 13].

Although the photovoltaic devices based on single-crystal silicon are the most successful ones, the high cost of manufacturing the single-crystal silicon has made them expensive. This is one of the main reasons because of why single-crystal solar cell technology has largely remained beyond the reach of developing countries [14, 15]. So, CdTe-based thin-film solar technology was developed as a cost-effective alternative for single-crystal silicon solar cells. Initially, NREL (USA) reported an efficiency of about 16.5% in CdTe solar cells [16] Since then, a significant increase in efficiency has been achieved (from 16.5 to 22%) through extensive research [17, 18].

The CdTe films can be deposited on different substrates such as glass, FTO, ITO, etc., depending upon the device requirements [19–21]. Both physical and chemical techniques have been employed to obtain CdTe films [22–25]. However, the chemical deposition of CdTe has many bottlenecks such as lack of stoichiometry, instability of tellurium atoms, and the formation of excess oxygen atoms

\*Corresponding author, E-mail: kgowrishrao@gmail.com; gk.rao@manipal.edu

[26]. Among the physical techniques, thermal evaporation has been a very popular choice. In this technique, uniform CdTe films can be easily prepared on different types of substrates. The method also offers relatively high deposition rates and minimum contamination. The cost of production is also low compared to other high-end physical techniques [27, 28].

Although several reports are available on thermally evaporated CdTe thin films, detailed studies of structural, electrical and photoresponse properties are yet to be undertaken. Most of the published work on CdTe films has focused on a very narrow range of thickness without offering any justification for the choice of such a narrow range [29, 30]. In the present work, we have investigated the properties of CdTe films with a broad range of thicknesses. The optimum thickness of CdTe has been determined through detailed structural, optical, electrical, and photo response studies.

## 2. Experimental details

The CdTe thin films were deposited on glass substrates by thermal evaporation technique. Before the preparation of the films, glass substrates were thoroughly cleaned for better adhesion. Initially, the substrates were immersed in dilute hydrochloric acid for 24 h. After that, the substrates were rinsed in acetone and distilled water for 10 min and finally dried.

A pre-determined amount of CdTe powder (99.99% purity, from Sigma-Aldrich) was taken in a molybdenum boat for deposition. The glass substrates were placed on the substrate holder directly above the molybdenum boats. The setup is placed inside a vacuum chamber and the molybdenum boat was resistively heated (under a residual pressure of  $10^{-6}$  Torr) until the CdTe powder is completely evaporated. The schematic diagram of the thermal evaporation setup is shown in Fig. 1.

The films thus obtained were subjected to detailed structural, optical, and electrical characterization. The structural and morphological properties of the films were investigated by Rigaku Miniflex X-ray Diffraction (XRD) and Oxford Scanning electron microscope (SEM). The optical, photoluminescence, and electrical properties of the films were studied by Shimadzu UV-VIS-NIR spectrometer, Hitachi Fluorescence Spectrophotometer, and Hall Effect measurement setup, respectively.

The spectral response of CdTe film was analyzed by HOLMARC<sup>TM</sup> Quasar Monochromator setup with a 150 W Xenon lamp. The photocurrent of the film was measured with the help of the Keithley meter.

## 3. Results and discussions

The thickness of the films was determined by the gravimetric method and later verified by a profilometer and SEM cross section image. The thickness of the obtained film samples ranged from 350 to about 1150 nm.

### 3.1. Structural properties

The thermally evaporated CdTe films were found to be polycrystalline with a cubic phase. The peaks corresponding to (111), (220), and (311) planes were visible in the XRD patterns (Fig. 2). The intensity of the prominent (111) peak increased with the film thickness up to 950 nm but then decreased slightly in the case of 1150 nm films. This behavior may be attributed to the lack of texture and discontinuity in the films.

The crystallite size and other microstructural parameters were determined from the XRD patterns. The well-known Scherrer formula was used to determine the crystallite size ( $D$ ) [31]. The formula can be written as,

$$D = \frac{0.9\lambda}{\beta \cos \theta} \quad (1)$$

where  $\lambda$  is the wavelength used (CuK $\alpha$ , i.e., 1.54 Å),  $\beta$  and  $\theta$  are the full-width at half maxima of the peaks correspond to Bragg's angle respectively. The values of ' $D$ ' are tabulated in.

The crystallite size of the films was found to increase with thickness up to 950 nm. The improvement in crystallinity was due to the reduction in the grain boundaries. At lower thicknesses, the atoms impinging on the substrate are concise and adhere to one zone of the surface rather than getting incorporated with the adjacent grains [32, 33]. However, as the thickness increases, the adjacent grains would get assimilated to form larger grains. The improvement in crystallinity also depends on the mobility of the deposited atoms on the surface. The higher mobility of the atoms results in the larger cluster formation with uniformly distributed crystallites. In thermal evaporation, more and more atoms get uniformly settled on the surface of the substrate with the increase of thickness. Also, at lower thicknesses, the dislocation of the atoms occurs more often compared to films of a higher thickness value (Table 1). The crystallite size was found to saturate at a thickness of around 950 nm. Further increase in thickness did not cause any improvement in the crystallite size. This behavior is typical of thermally evaporated films. It is not possible to have indefinitely higher crystallite size in thermally evaporated films just by increasing thickness. Hence, the crystallite size in the 1150 nm films was found to be lower compared to that of the 950 nm film. Besides, in thermal evaporation, the formation of the films takes

**Fig. 1** The schematic diagram of thermal evaporation setup

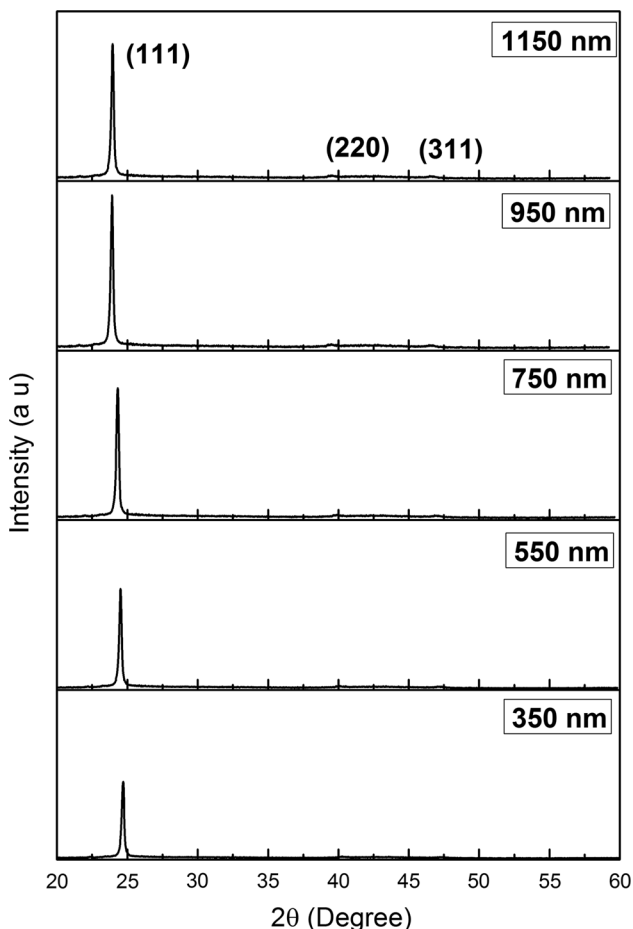
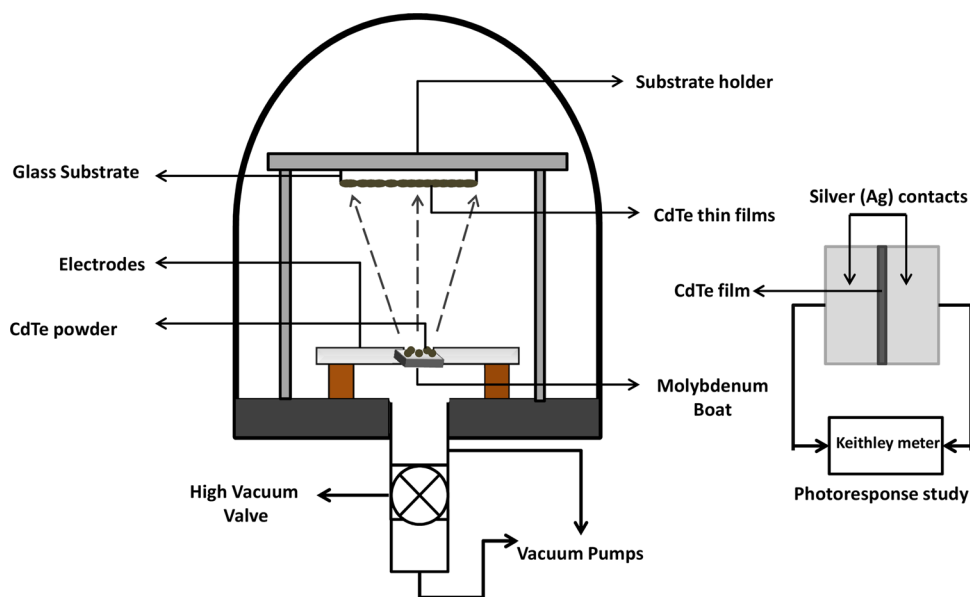


**Fig. 2** The XRD patterns of CdTe thin films with different thickness

place in one crystallographic direction. This tends to lower the surface energy density, which is tabulated in Table 2.

The dislocation density of the CdTe thin films was determined from the following formula [34].

$$\delta = \frac{1}{D^2} \tag{2}$$

The value of crystallite size was further verified by Williamson–Hall (W–H) plot [35], as shown in Fig. 3. The linear graph gives the idea of strain developed in the deposited films according to the relation,

$$\beta \cos \theta = \frac{0.9\lambda}{D} + 4\epsilon \sin \theta \tag{3}$$

The W–H plot describes the average crystallite size from all the XRD peaks and the strain induced due to peak broadening. The crystallite size ( $D$ ) and the strain ( $\epsilon$ ) obtained from the y-intercept and slope of the above relation are tabulated in Tables 1 and 2.

The lattice constants of the films were also determined for different thicknesses. The well-known Bragg’s equation gives the relation between interplanar spacing ( $d$ ) and wavelength ( $\lambda$ ) [36].

$$\text{i.e } 2d \sin \theta = n\lambda \tag{4}$$

The lattice constant ‘ $a$ ’ for cubic phase with miller indices ( $h k l$ ) can be calculated from the following relation,

$$a = d\sqrt{h^2 + k^2 + l^2} \tag{5}$$

As the thickness increased, the lattice constants of the CdTe films were found to approach the bulk values (Table 2). The change in the lattice constants can be attributed to the decrease in the surface energy density, which tends to dislocate the films from the surface. For the thickness of 950 nm, the lattice constant was found to be

**Table 1** The crystallite size of CdTe films at different thickness

Thickness (nm)	Crystallite size $D$ (nm)		Dislocation density $\delta \times 10^{15}$ ( $\text{m}^{-2}$ )
	From Scherrer formula	From W-H Plot	
350	19.89	18.72	2.52
550	29.49	29.17	1.14
750	37.45	36.84	7.12
950	38.80	38.43	6.64
1150	35.39	34.91	7.74

6.47 Å. The slight residual mismatch from the bulk value is due to disorientation and the presence of defects in the films.

The lattice constants of the CdTe thin films were verified by Nelson–Riley (N–R) plot (Table 2). The N–R plot yields better accuracy by accommodating the effects of peak broadening in the polycrystalline films [37]. The N–R function can be written as follows:

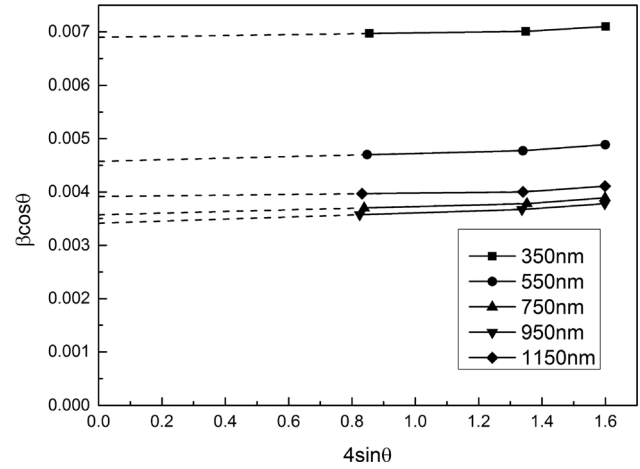
$$e(\theta) = \frac{1}{2 \left[ \frac{\cos^2 \theta}{\theta} + \frac{\cos \theta}{\tan \theta} \right]} \quad (6)$$

The plot of  $e(\theta)$  versus ' $a$ ' was found to be linear (Fig. 4). The values of the lattice constant were obtained by extrapolating this linear graph.

The polycrystalline nature of the films invariably results in stain-induced peak broadening. Furthermore, the

**Table 2** The results obtained from XRD analysis of CdTe films

Thickness (nm)	(hkl)	Lattice constant $a$ (Å)		$\varepsilon \times 10^{-3}$	$S \times 10^8$ ( $\text{N/m}^2$ )	$U \times 10^6$ ( $\text{J/m}^3$ )
		From XRD	From N–R plot			
350	111	6.25	6.25	8.15	15.11	28.55
	220	6.24				
	311	6.24				
550	111	6.29	6.29	5.54	12.46	19.43
	220	6.29				
	311	6.28				
750	111	6.38	6.38	4.41	7.12	5.39
	220	6.37				
	311	6.37				
950	111	6.47	6.47	4.33	0.46	0.03
	220	6.46				
	311	6.47				
1150	111	6.40	6.41	4.69	4.31	2.32
	220	6.41				
	311	6.40				

**Fig. 3** The W–H plot of CdTe thin films with different thickness

dislocation in the films may be present in one crystallographic direction, which causes stress [38]. The strain produced in the films was determined from Eq. (3) and tabulated in Table 2. The improved crystallite size at higher thickness results in a corresponding decrease in strain (up to the film thickness of 950 nm). At 1150 nm, a slight increase in the broadening of the peak was observed as a direct consequence of the decrease in crystallite size.

The stress developed in the films was determined by the relation,

$$S = \frac{(a_0 - a)Y}{2a_0\sigma} \quad (7)$$

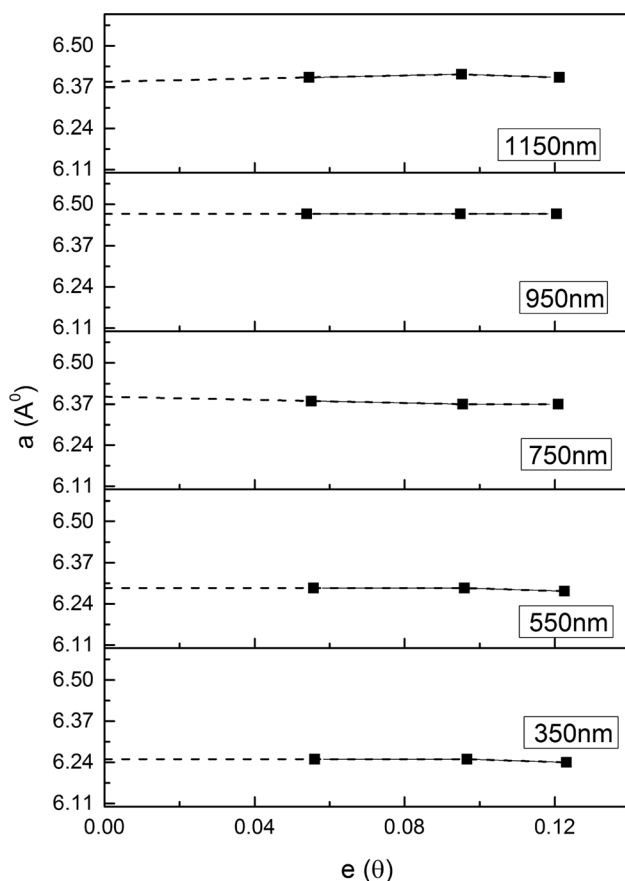


Fig. 4 The N-R plot of CdTe thin films with different thickness

where  $a_0$  and  $a$  are the lattice constants of CdTe for bulk and thin-film form.  $Y$  and  $\sigma$  are Young's modulus and Poisson's ratio of the CdTe thin films, respectively. For the calculations, the values of  $Y = 4 \times 10^{10}$  N/m<sup>2</sup> and  $\sigma = 0.469$  were used [39]. The stress in the CdTe thin films was also found to decrease with thickness up to 950 nm (Table 2). At lower thickness, the dislocation in the CdTe films was found to be high. Since the polycrystalline films are in the form of a collection of grains (separated from each other by grain boundary regions), the dislocation of grains is expected at higher stress levels.

The elastic surface energy density was calculated using the following formula [40].

$$U = \frac{S^2}{2Y} \quad (8)$$

The decrease in elastic surface energy density with the thickness (Table 2) can be attributed to improvement in crystallite size and reduced stress. The slight decrease in the crystallite size (at the film thickness of 1150 nm) would increase the surface energy density.

The SEM image showed uniform surface coverage in the films. The films were devoid of any macroscopic

imperfections. The EDS analysis showed that the composition of the films deviated marginally from stoichiometry. However, the composition changed with the thickness (Table 3). The thermal evaporation technique is notorious for producing non-stoichiometric films. The difference in the vapor pressures of the constituent elements (Cd and Te) results in an asymmetrical supply of atoms of the two species at the substrate. The films with a thickness of 950 nm, were found to possess a nearly stoichiometric composition.

### 3.2. Optical properties

The optical properties of the films are mainly governed by the movement of electrons and the presence of defects in the films. Since the crystal structure has a strong bearing on the free movement of electrons, the optical properties of the films may also vary with the thickness. The optical absorbance spectra were recorded in the wavelength range of 450–1100 nm. The films were found to have high absorption in the near-infrared (NIR) region as reported previously by other research groups [41, 42]. The absorbance of the films increased initially with thickness up to 1150 nm as shown in (Fig. 5a). The improvement in the crystallinity tends to reduce the scattering loss. Therefore, absorbance increased with the crystallite size of the CdTe films. The absorption coefficient  $\alpha$  and the energy bandgap of the films can be determined from the absorbance spectra using the relation [43].

$$\alpha hv = A(hv - E_g)^n \quad (9)$$

In the relation, the value of  $n$  indicates the nature of transition ( $n = 1/2$  for direct and  $n = 2$  for indirect). In the present case, the plot of  $(\alpha hv)^2$  versus  $hv$  was found to be linear suggesting that the bandgap is direct. The value of the energy bandgap was found by extrapolating the linear part of the graph to meet the  $x$ -axis (Fig. 5b).

The energy bandgap of the films was also found to vary with thickness. When the thickness increased, the absorption edge of the films shifted toward the higher wavelengths. The bandgap of the films varied from 1.52 to 1.45 eV which agrees well with the earlier reports [44, 45].

The extinction coefficient of the CdTe thin films was calculated from the relation [46]

$$k = \frac{\alpha \lambda}{4\pi} \quad (10)$$

The variation of extinction coefficient with film thickness is shown in Fig. 6a. The increase in crystallite size leads to a reduction in the defects due to the reduced grain boundary region. This is chiefly responsible for the variation of the extinction coefficient with thickness.

**Table 3** The composition of the CdTe films

Thickness (nm)	The atomic percentage of cadmium	The atomic percentage of tellurium
350	51.12	48.88
550	50.40	49.60
750	50.14	49.86
950	50.02	49.98
1150	50.21	49.79

The thickness of the films was also found to influence the refractive index. The refractive index can be determined from the absorbance spectra using the relation [47].

$$R = 1 - (A + T) \quad (11)$$

$$n = \frac{1+R}{1-R} + \sqrt{\left[\left(\frac{4R}{1-R^2}\right) - k^2\right]} \quad (12)$$

where  $R$  and  $k$  are the reflectance and extinction coefficient of the CdTe films, respectively. The refractive index was found to increase with thickness, as shown in Fig. 6b. The improvement in crystallinity and the marginal changes in the composition of the films have influenced their refractive index.

The optical conductivity of the films was determined from the following relation [48].

$$\sigma = \frac{\alpha nc}{4\pi} \quad (13)$$

The graph of  $\sigma$  versus  $h\nu$  demonstrates the effect of the thickness on the optical conductivity of the films. The variation of optical conductivity with thickness is shown in Fig. 6c. This is a direct consequence of the corresponding variation in the absorbance of the films due to the increased crystallite size.

The stress and the fine grain structure are the main sources of the defects present in the films. To quantify the presence of defects, the Urbach energy was calculated using the following relation [49].

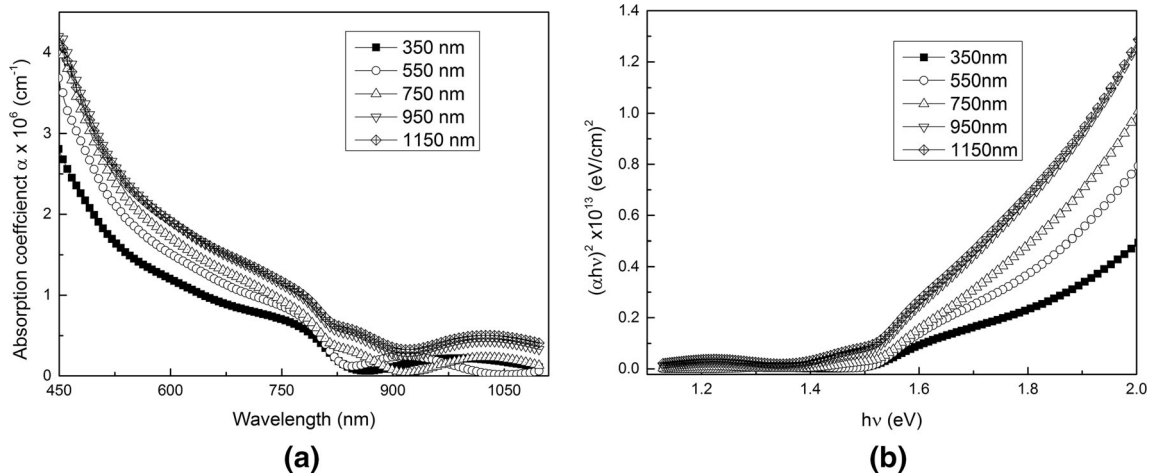
$$\alpha = \alpha_0 \exp \frac{h\nu}{E_u} \quad (14)$$

The plot  $\ln(\alpha)$  versus  $h\nu$  was found to be linear (Fig. 7a) and the inverse of its slope was obtained as Urbach energy ( $E_u$ ). The Urbach energy was found to decrease with the increase in the thickness of the films (Fig. 7b). The reduction in Urbach energy indicates the reduction in defects due to the improvement in crystallinity. But for the 1150 nm sample, a slight rise in the Urbach energy was observed which is due to the marginal decrease in the crystallite size.

The photoluminescence (PL) spectra of the films were recorded with the excitation wavelength of 550 nm. The PL spectra (Fig. 8a) showed two peaks whose intensity increased with thickness. The peaks also shifted toward the higher wavelengths. The smaller peak ( $\sim 600$  nm) corresponds to the electron-hole recombination of the tellurium atoms [50]. The prominent peak ( $\sim 780$  nm) is due to the band-edge emission of the films [51, 52]. The Commission International De I-Eclairage (CIE)-1931 chromaticity diagram was plotted for CdTe films (Fig. 8b). The films showed emission in the orange region with a marginal deviation in the  $x$ - $y$  coordinates. The  $x$ - $y$  coordinates of the CIE plot were found to be  $x = 0.582$ ,  $y = 0.379$  and  $x = 0.605$ ,  $y = 0.389$  for the 350 nm and 950 nm thickness respectively.

### 3.3. Electrical properties

Silver (Ag) ohmic contacts were deposited on the films by vacuum deposition. A Hall Effect setup (with Vander Pauw

**Fig. 5** (a) Absorbance spectra and (b) Tauc plot of CdTe films



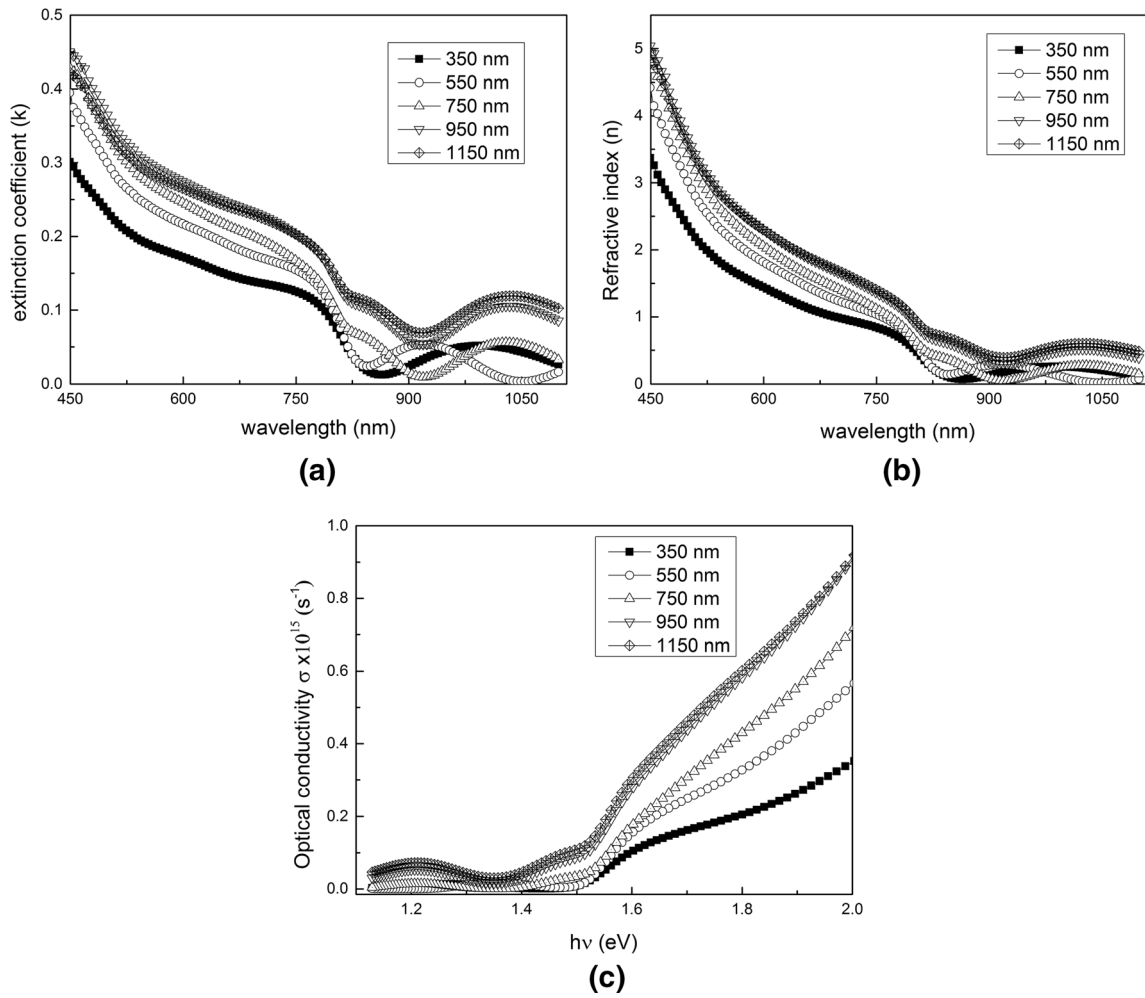


**Fig. 6** The optical properties of CdTe thin films: (a) extinction coefficient, (b) refractive index, (c) optical conductivity

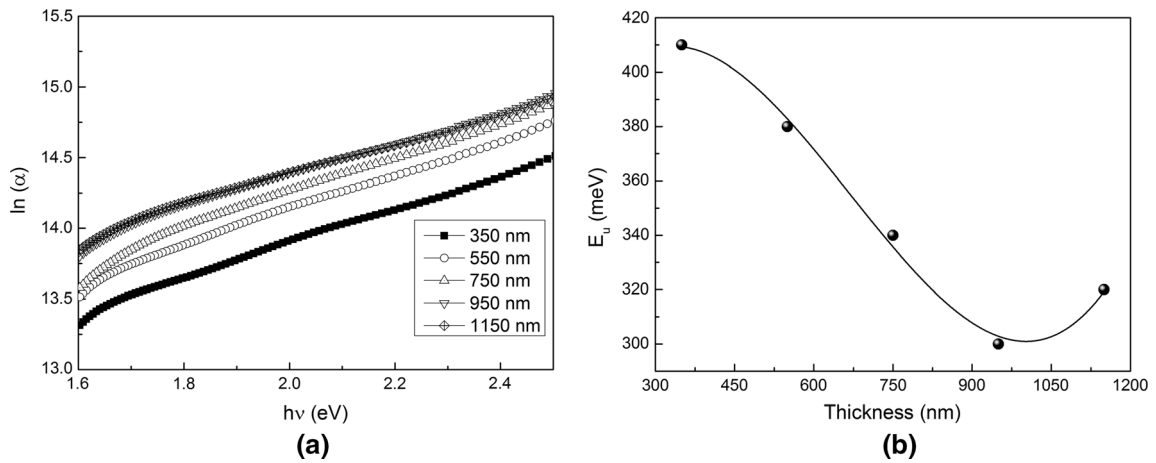


**Fig. 7** (a)  $\ln(\alpha)$  versus  $h\nu$  plot and (b) the variation of Urbach energy

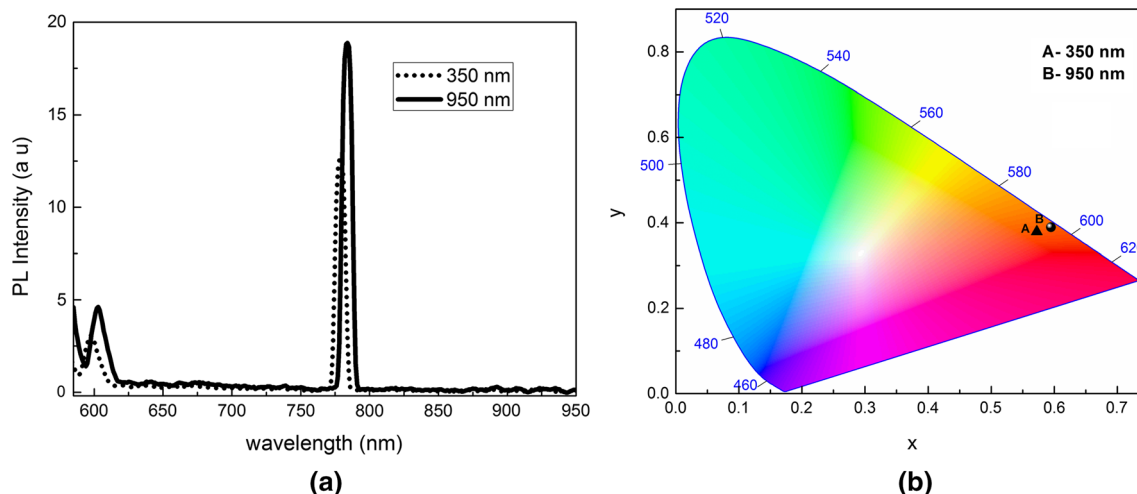


**Fig. 8** The (a) PL spectrum and (b) chromaticity diagram of CdTe films

**Table 4** The electrical properties of CdTe films

Thickness (nm)	Resistivity $\times 10^2$ ( $\Omega$ cm)	Carrier concentration $\times 10^{15}$ ( $\text{cm}^{-3}$ )	Mobility ( $\text{cm}^2 \text{V}^{-1} \text{s}^{-1}$ )
350	11.4	1.3	35.1
550	9.3	2.2	67.4
750	8.2	3.4	94.2
950	5.7	4.8	120.5
1150	6.1	4.1	97.4

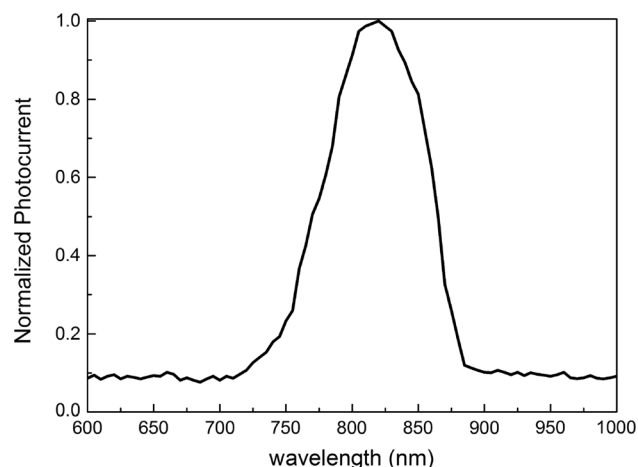


**Fig. 9** The spectral response of CdTe film (950 nm thickness)

geometry) was used to find the resistivity, carrier concentration, and mobility of the films (Table 4).

All the films were found to be of p-type. The resistivity of the CdTe thin films decreased with thickness. At lower thicknesses, the pronounced scattering effect impede the

conduction of the electrons. The larger grain boundary regions (due to smaller average grain size) might also contribute to the electrical resistivity. When the film thickness increases, the scattering effect becomes less effective. The grain boundaries will also reduce resulting in better electrical conduction. But for the 1150 nm sample, the resistivity was found to increase slightly due to the reduction in crystallite size.

The improvement in the crystallinity also minimizes the formation of carrier traps in the films. This results in the increase of carrier concentration (from  $1.3 \times 10^{15}$  to  $4.8 \times 10^{15} \text{ cm}^{-3}$ ) and electron mobility of the films (up to the thickness of 950 nm). Thus, the CdTe films of a thickness of about 950 nm showed optimum structural, optical, and electrical properties. A similar result has been reported by Paudel et al. [53].

The spectral response of the films (thickness 950 nm) was analyzed at wavelengths ranging from 600 to 1000 nm. The white light from a 150 W Xenon lamp was passed through a computer-controlled, high precision, grating monochromator to get monochromatic light of desired wavelengths. This monochromatic light was allowed to fall on the CdTe film. The whole setup was kept in a dark chamber and the photocurrent was measured (with a 5 V bias) by a computer interfaced Keithley meter.

The photocurrent of the film was found to be high around the wavelength of 820 nm (Fig. 9) which corresponds to the band gap of the films. When the light of energy equal to (or higher than) the band gap is incident on the material, electron-hole pairs are generated [54]. The samples of 950 nm thickness were found to yield the highest photocurrent among all the analyzed samples.



#### 4. Conclusions

The cadmium telluride (CdTe) thin films of different thicknesses were deposited on glass substrates by thermal evaporation technique. The XRD patterns showed the presence of a cubic phase in the films with a preferred orientation along the (111) plane. Considerable improvement in the crystal structure was observed with the increase in thickness. The films showed high absorption in the NIR region. The direct energy bandgap of the films varied marginally with the thickness. The Urbach energy reduced with the increase in thickness suggesting a significant reduction in defects. The photoluminescence spectra of the films showed a prominent peak corresponding to the band-edge emission, whereas the CIE plot showed that the CdTe films have emissions in the orange region. The films were found to be p-type. The resistivity of the films decreased with the increase in thickness owing to the improvement in the crystal structure.

The carrier concentration of the films was found to be high for 950 nm thickness. The films yield maximum photocurrent at 820 nm. Thus, the analysis of structural, optical, and electrical properties has shown that the thickness of 950 nm is optimum for thermal evaporated CdTe films as these films possess larger crystallite size, higher absorption coefficient, lower resistivity, and higher carrier concentration.

**Acknowledgements** The authors are thankful to the Manipal Institute of Technology (MAHE, Manipal) for providing the research facility.

**Authors' contribution** AVK contributed to major experimental work and preparation of the manuscript; PK provided assistance in film growth and characterization work; GRK performed supervision of research work and review of the manuscript.

**Funding** Manipal Institute of Technology, MAHE, Manipal. (Internal funding, No sanction number required).

**Availability of data and material** Data cannot be made available at this point as it is part of the ongoing research. Code availability Not Applicable.

#### Declarations

**Consent for publication** All authors have provided their consent for publication.

**Conflict of interest** Authors declare that they have no conflict of interest/competing interests.

**Ethics statement** Not Applicable (The work is not in the field of biological sciences).

#### References

- [1] K Seshan *Handbook of Thin-Film Deposition Processes and Techniques* (New York: Noyes Publications) (2002)
- [2] H Frey and H R Khan *Handbook of Thin Film Technology* (Berlin, Heidelberg: Springer) (2015)
- [3] K J Hsiao *Solar Energy Mater. Solar Cells* **120** 647 (2014).
- [4] A Bosio, N Romeo, S Mazzamuto and V Canevari *Prog. Cryst. Growth Charact. Mater.* **52** 247 (2006).
- [5] X Wen, Z Lu, X Sun, Y Xiang, Z Chen, J Shi, I Bhat, G-C Wang, M Washington and T-M Lu *ACS Appl. Energy Mater.* **3** 4589 (2020).
- [6] M S Hossain, K S Rahman, M R Karim, M O Aijaz, M A Dard, M A Shard, H Misrana and N Amin *Solar Energy* **180** 559 (2019).
- [7] X Li, K Shen, Q Li, Y Deng, P Zhu and D Wang *Solar Energy* **165** 27 (2018).
- [8] K S Rahman, M N Harif, H N Rosly, M I Bin Kamaruzzaman, M Akhtaruzzaman, M Alghoul, H Misran and N Amin *Results Phys.* **14** 102371 (2019).
- [9] V V Brus, P D Maryanchuk, M I Ilashchuk, J Rappich, I S Babichuk and Z D Kovalyuk *Solar Energy* **112** 78 (2015).
- [10] L I Nykyruy, R S Yavorskyi, Z R Zapukhlyak, G Wisz and P Potera *Opt. Mater.* **92** 319 (2019).
- [11] V K Ashith, K Priya and G K Rao *Physica B Condens. Matter* **614** 413025 (2021).
- [12] A Pidluzhna, K Ivaniuk, P Stakhira, Z Hotra, M Chapran, J Ulanski, O Tynkevych, Y Khalavka, G V Baryshnikov and B F Minaev *Dyes Pigments* **162** 647 (2019).
- [13] Y Wang, X Huang, D Wu, R Zhuo, E Wu, C Jia, Z Shi, T Xu, Y Tian and X Li *J. Mater. Chem. C* **6** 4861 (2018).
- [14] A Haeri *J. Mater. Sci. Mater. Electron.* **28** 18183 (2017).
- [15] J Ramanujam, D M Bishop, T K Todorov, O Gunawan, J Rath, R Nekovei, E Artegiani and A Romeo *Prog. Mater. Sci.* **110** 100619 (2020).
- [16] T D Lee and A U Ebong *Renewable and Sustainable Energy Reviews* **70** 1286 (2017).
- [17] H S Ullal, K Zweibel and B Von Roedern *IEEE Photovol. Special. Conf.* **1** 472 (2002).
- [18] I M Dharmadasa and A A Ojo *J. Mater. Sci. Mater. Electron.* **28** 16598 (2017).
- [19] A M A Hakeem, H M Ali, M M A El-Raheem and M F Hasaneen *Optik* **225** 165390 (2021).
- [20] E Hasani and M Kamalian *J. Electron. Mater.* **48** 4283 (2019).
- [21] C Doroody, K S Rahman, S F Abdullah, M N Harif, H N Rosly, S K Tiong and N Amin *Results Phys.* **18** 103213 (2020).
- [22] P Gu, X Zhu, J Li, H Wu and D Yang *J. Mater. Sci. Mater. Electron.* **29** 14635 (2018).
- [23] D Wang, Y Yang, T Guo, X Xiong, Y Xie, K Li, B Li and M Ghali *Solar Energy* **213** 118 (2021).
- [24] A Arce-Plaza, J A Andrade-Arvizu, M Courel, J A Alvarado and M Ortega-Lopez *J. Analyt. Appl. Pyrolysis* **124** 285 (2017).
- [25] T M Demiriz and A Peksoz *J. Mater. Sci. Mater. Electron.* **30** 8645 (2019).
- [26] G Hodes *Chemical Solution Deposition of Semiconductor Thin Films* (New York: Marcel Dekker Inc) (2002)
- [27] N A Khan, K S Rahman, K A Aris, A M Alia, M Halina Misran, S Akhtaruzzaman, K Tiong and N Amin *Solar Energy* **173** 1051 (2018).
- [28] P K K Kumarasinghe, A Dissanayake, B M K Pemasiri and B S Dassanayake *Mater. Res. Bull.* **96** 188 (2017).
- [29] S Chander and M S Dhaka *Physica E Low Dimens. Syst. Nanostruct.* **76** 52 (2015).
- [30] S A Fadaam, M H Mustafa, A H A AlRazaK and A A Shihab *Energy Procedia* **157** 635 (2019).

- [31] A L Patterson *Phys. Rev.* **56** 978 (1939).
- [32] L Eckertova *Physics of Thin Films* (New York: Springer) (1977)
- [33] V K Ashith and E Deepak *J. Mater. Sci. Mater. Electron.* **32** 10028 (2021).
- [34] T Shintani and Y Murata *Acta Materialia* **59** 4314 (2011).
- [35] G K Williamson and W H Hall *Acta Mater.* **1** 22 (1953).
- [36] W L Bragg *Proc. Camb. Philos. Soc.* **17** 43 (1913).
- [37] J B Nelson and D P Riley *Proc. Phys. Soc.* **53** 160 (1945).
- [38] G Abadias, E Chason, J Keckes, M Sebastiani, G B Thompson, E Barthel, G L Doll, C E Murray and C H Stoessel *J. Vac. Sci. Technol. A Vac. Surf. Films* **36** 020801 (2018).
- [39] S Adachi *Properties of Group-IV III-V and II-VI Semiconductors* (New York: Wiley) (2005)
- [40] K Wasa, M Kitabatake and H Adachi *Thin Film Materials Technology* (Heidelberg Berlin: Springer) (2004)
- [41] P K K Kumarasinghe, A Dissanayake, B M K Pemasiri and B S Dassanayake *Mater. Sci. Semicond. Process.* **58** 51 (2017).
- [42] S Chander and M S Dhaka *Results in Physics* **8** 1131 (2018).
- [43] B D Viezbicke, S Patel, B E Davis and D P Birnie *Phys. Status Solidi B* **252** 1700 (2015).
- [44] S Lalitha, R Sathyamoorthy, S Senthilarasu, A Subbarayan and K Natarajan *Solar Energy Mater. Solar Cells* **82** 187 (2004).
- [45] E R Shaaban, N Afify and A El-Taher *J. Alloys Compd.* **482** 400 (2009).
- [46] E Hasani and D Raoufi *Mater. Res. Express* **5** 046413 (2011).
- [47] A A Al-Ghamdi, S A Khan, A Nagat and M S Abd El-Sadek *Opt. Laser Technol.* **42** 1181 (2010).
- [48] J I Pankove *Optical Processes in Semiconductors* (New York: Dover Publications Inc) (1975)
- [49] S J Ikhmayies and R N Ahmad-Bitar *Journal of Materials Research and Technology* **2** 221 (2013).
- [50] S N Moger, D U Shanubhogue, R Keshav and M G Mahesha *Superlatt. Microstruct.* **142** 106521 (2020).
- [51] T M Razykov, K M Kuchkarov, C S Ferekides, B A Ergashev, R T Yuldoshov, N Mamarasulov and M A Zufarov *Solar Energy* **144** 411 (2017).
- [52] I M Dharmadasa, O K Echendu, F Fauzi, N A Abdul-Manaf, H I Salim, T Druffel, R Dharmadasa and Lavery *J. Mater. Sci. Mater. Electron.* **26** 4571 (2015).
- [53] N R Paudel, K A Wieland and A D Compaan *Solar Energy Mater. Solar Cells* **105** 109 (2012).
- [54] A D Dhondge, S R Gosavi, N M Gosavi, C P Sawant, A M Patil, A R Shelke and N G Deshpande *World J. Condens. Matter Phys.* **5** 1 (2015).

**Publisher's Note** Springer Nature remains neutral with regard to jurisdictional claims in published maps and institutional affiliations.

Springer Nature or its licensor holds exclusive rights to this article under a publishing agreement with the author(s) or other rightsholder(s); author self-archiving of the accepted manuscript version of this article is solely governed by the terms of such publishing agreement and applicable law.